

~~CONFIDENTIAL~~

Copy 5
RM A54D22

NACA RM A54D22



RESEARCH MEMORANDUM

INVESTIGATION OF THE NORMAL FORCE ACCOMPANYING THRUST-
AXIS INCLINATION OF THE NACA 1.167-(0)(03)-058 AND THE
NACA 1.167-(0)(05)-058 THREE-BLADE PROPELLERS
AT FORWARD MACH NUMBERS TO 0.90

By Fred A. Demele and William R. Otey

Ames Aeronautical Laboratory
Moffett Field, Calif.

CLASSIFICATION CHANGED

UNCLASSIFIED

LIBRARY COPY

To _____

NACA Rec Abs

7 RN-126

effective

JUN 23 1954

By authority of _____ Date *Apr 15, 1958*

AM 5-8-58

LANGLEY AERONAUTICAL LABORATORY
LIBRARY, NACA
LANGLEY FIELD, VIRGINIA

CLASSIFIED DOCUMENT

This material contains information affecting the National Defense of the United States within the meaning of the espionage laws, Title 18, U.S.C., Secs. 793 and 794, the transmission or revelation of which in any manner to an unauthorized person is prohibited by law.

NATIONAL ADVISORY COMMITTEE FOR AERONAUTICS

WASHINGTON

June 23, 1954

~~CONFIDENTIAL~~



U
NACA RM A54D22

NATIONAL ADVISORY COMMITTEE FOR AERONAUTICS

RESEARCH MEMORANDUM

INVESTIGATION OF THE NORMAL FORCE ACCOMPANYING THRUST-
AXIS INCLINATION OF THE NACA 1.167-(0)(03)-058
AND THE NACA 1.167-(0)(05)-058 THREE-BLADE
PROPELLERS AT FORWARD MACH NUMBERS TO 0.90

By Fred A. Demele and William R. Otey

SUMMARY

An investigation has been conducted to determine experimentally the normal force of the NACA 1.167-(0)(03)-058 and the NACA 1.167-(0)(05)-058 three-blade propellers and to ascertain the agreement of the measured normal force with a theoretical method developed herein. The propeller thrust and normal force were measured with the thinner propeller for a range of blade angles and angles of attack at forward Mach numbers from 0.60 to 0.90. For the thicker propeller, similar measurements were made at forward Mach numbers of 0.082 and 0.123.

The results indicated that the normal-force coefficient generally increased with increasing thrust coefficient at Mach numbers below 0.70 and remained essentially constant at the higher Mach numbers. With few exceptions, the increase in normal-force coefficient with upflow angle at the 0.7 propeller radius was essentially linear. Increasing propeller blade angle increased the normal-force coefficient for a given value of thrust coefficient and angle of attack.

Comparison between the normal force calculated by a method developed herein and that measured experimentally indicated excellent agreement for a representative high Mach number condition. At low forward speeds the theoretical method predicted the variation with thrust coefficient and blade angle with fair accuracy, but consistently underestimated the effect of thrust-axis inclination.

INTRODUCTION

The gas-turbine engine driving a conventional or supersonic propeller appears to be an attractive propulsion system for certain classes of long-range airplanes designed to fly at moderately high

~~CONFIDENTIAL~~

subsonic speeds. In the aerodynamic design of such a turboprop airplane, consideration must be given to the direct effects of the propellers on the airplane stability.

A propeller produces forces normal to the thrust axis whose variation with angle of attack is destabilizing for a conventional tractor airplane having the propellers ahead of the center of gravity. The magnitude of these propeller forces must be determined either by experiment or by a satisfactory theoretical method. The experimental normal-force characteristics of propellers designed to operate at high section Mach numbers and having large power-absorption capabilities have been virtually nonexistent. Among the several existing methods of calculating propeller normal force, Ribner's method (ref. 1) has perhaps been most widely accepted. This acceptance has been fostered by the fact that it affords a solution which has, heretofore, been satisfactory and requires little more than a knowledge of blade shape. However, the method does not completely account for the nonuniformity of the flow field due to the presence of a nacelle, fuselage, or wing, nor does it adequately account for compressibility effects, particularly when the helical Mach numbers are high.

The present investigation includes measurements of normal force for two, three-blade propellers of high solidity, differing only in thickness, at forward Mach numbers up to 0.90 and a comparison of measured and calculated results. The theoretical method used for the calculations is developed herein and is based on the concept of oscillating aerodynamic forces associated with propeller blades operating in an inclined flow field. The authors are indebted to Messrs. Vernon L. Rogallo and John L. McCloud III, of the Ames Aeronautical Laboratory, for their contribution to the theory.

NOTATION

- A upflow angle, angle of local flow at 0.7 propeller radius and at the horizontal center line of the propeller plane, measured in a vertical plane with respect to the thrust axis
- A' local upflow angle
- b blade width
- B number of blades
- c_d blade-section drag coefficient, $\frac{\text{section drag}}{\frac{1}{2} \rho W^2 b}$

c_{f_Q}	blade-section torque-force coefficient, $\frac{\text{section torque force}}{qb}$
c_l	blade-section lift coefficient, $\frac{\text{section lift}}{\frac{1}{2} \rho W^2 b}$
C_N	propeller normal-force coefficient, $\frac{N}{qS}$
D	propeller diameter
$\frac{b}{D}$	blade width ratio
f_n	blade-section normal force, normal to thrust axis
f_Q	blade-section torque force
h	maximum thickness of blade section
$\frac{h}{b}$	blade thickness ratio
J	advance ratio, $\frac{V}{nD}$
K	Goldstein correction factor for finite number of blades
M	free-stream Mach number
n	propeller rotational speed
N	propeller normal force, normal to thrust axis
q	free-stream dynamic pressure, $\rho \frac{V^2}{2}$
r	blade-section radius
r_s	spinner radius
R	free-stream Reynolds number per foot, $\rho \frac{V}{\mu}$
R_t	propeller-tip radius
S	propeller disk area
T	thrust, measured parallel to free stream
T_c	thrust coefficient, $\frac{T}{\rho V^2 D^2}$

V	free-stream velocity
V'	local forward velocity
V_a	axial interference velocity
V_i	resultant interference velocity
V_r	rotational interference velocity
w	rearward displacement velocity of helical vortex surface at infinity
\bar{w}	ratio of displacement velocity to component of local forward velocity parallel to thrust axis
W	blade-section helical velocity considering induced effects
W_0	blade-section helical velocity neglecting induced effects
x	fraction of tip radius, $\frac{r}{R_t}$
x_s	ratio of spinner radius to tip radius, $\frac{r_s}{R_t}$
α	angle of attack of the thrust axis with respect to the free-stream direction
α'	blade-section angle of attack
α_1	propeller induced angle of inflow
β	blade angle at 0.7 radius
β'	blade angle
γ	$\tan^{-1} \left(\frac{c_d}{c_l} \right)$
μ	absolute viscosity
ρ	free-stream density
σ	propeller solidity, $\frac{Bb}{2\pi r}$
ϕ	$\phi_0 + \alpha_1$
ϕ_0	$\tan^{-1} \left(\frac{V' \cos A'}{\pi n D x + V' \sin A' \sin \Omega} \right)$
Ω	angular position about the thrust axis, in the direction of propeller rotation from the upper vertical position

MODEL AND APPARATUS

This investigation was conducted in the Ames 12-foot pressure wind tunnel. The apparatus and test methods described in reference 2 were used, although the nacelle assembly was modified slightly to permit measurement of isolated propeller-spinner characteristics. Figure 1 is a photograph of the assembly mounted in the wind tunnel, and a schematic drawing of the assembly is shown in figure 2. Coordinates of the body portion of the assembly are given in table I.

Nacelle Assembly

The primary structure of the nacelle assembly consisted of an electric motor and extension propeller shaft supported by a strut rigidly mounted to the framework of the six-component balance system. The secondary structure consisted of a fairing enclosing the primary structure. The fairing assembly was rigidly attached to the wind-tunnel floor structure and was independent of the primary structure. The secondary structure had no direct influence on the measured propeller forces, but did affect the flow field in the region of the propeller. A clearance gap was provided between the primary and secondary nacelle structure, as shown in figure 2, to prevent transmission of extraneous forces to the balance system. A concentric rubber membrane sealed the area between the primary and secondary nacelle structures, and static-pressure orifices on either side of the seal permitted the pressure forces acting on the rear of the primary nacelle structure to be determined.

Motor

The propeller was driven by an electric motor having a normal rating of 75 horsepower at 18,000 revolutions per minute. Continuous speed control of the motor was accomplished by means of a variable-frequency power supply. Motor-speed indication was provided by a frequency-measuring instrument connected to a variable-reluctance alternator located on the rear of the motor.

Spinner

The spinner used in this investigation had a maximum diameter of 4.20 inches and the NACA 1-series profile. The diameter at the plane of the propeller was 3.97 inches, or 28.3 percent of the propeller diameter,

and the length forward of the propeller plane was 5.00 inches. Coordinates of the spinner are given in table I. A clearance gap of 0.015 inch was provided between the spinner and the forward face of the extension shaft housing. Individual spinners were provided with blade cutouts corresponding to each blade angle. The gap between the blade and spinner was not sealed.

Propellers

The NACA 1.167-(0)(03)-058 three-blade propeller was a 1/12-scale model of a propeller designed to absorb 5000 horsepower with an efficiency of 75 percent at a forward Mach number of 0.83 and an altitude of 40,000 feet. The design value of advance ratio was 2.01 and the design blade angle at 0.70 radius was 46.3° .

The NACA 1.167-(0)(05)-058 propeller was identical to the NACA 1.167-(0)(03)-058 propeller, except that the blade thicknesses were greater by a factor of $5/3$ at all radial stations. This propeller was designed specifically to withstand the very high blade loadings accompanying low-speed operations in the wind tunnel at an air density of 6 atmospheres.

Additional design criteria for the two propellers may be found in reference 2. Blade-form curves are presented in figure 3. The propeller blades had NACA 16-series sections and were machined from heat-treated alloy steel.

TEST CONDITIONS

Propeller thrust, normal force, and rotational speed were measured for both the NACA 1.167-(0)(03)-058 and the NACA 1.167-(0)(05)-058 propellers. Data were obtained for the thicker propeller at Mach numbers of 0.082 and 0.123 for blade angles of 21° , 26° , and 31° throughout an angle-of-attack range from -3.92° to 15.68° . Data were obtained for the thin propeller at blade angles of 46° , 51° , and 56° throughout an angle-of-attack range from -3.92° to 5.88° at Mach numbers ranging from 0.60 to 0.90. The investigation was made at a Reynolds number per foot of 3,200,000 at the lower Mach numbers and 1,600,000 at Mach numbers of 0.60 and above.

REDUCTION OF DATA

Propeller Forces

Propeller force (i.e., thrust or normal force) as used herein is the difference between the force produced by the propeller-spinner combination and the nacelle forebody (i.e., that portion forward of nacelle station 3.25, table I) and the force produced by the spinner and nacelle forebody in the absence of the propeller at the same attitude, Mach number, and Reynolds number. Thrust is in the direction of the measured longitudinal force; whereas normal force is resolved from the measured lift and longitudinal force in a direction normal to the thrust axis. The forces were measured by the six-component balance system.

Seal-Pressure Correction

The pressures acting on either side of the concentric seal were measured, and the forces resulting from the measured pressures were adjusted for computational purposes to correspond to a reference pressure equal to the free-stream static pressure. The appropriate component of this pressure force was applied to the measured thrust for tests with the propeller operating and also with the propeller removed. Choice of free-stream static pressure for a reference pressure determined the net tare force but had no effect on either the propeller thrust or normal force as defined herein.

Tunnel-Wall Correction

The data have been corrected for the effect of tunnel-wall constraint on the velocity in the region of the propeller plane by the method of reference 3. The magnitude of the maximum correction applied to the data was 0.7 percent. The constriction effects, due to operating the propeller, were evaluated by the method of references 4 and 5 and were found to be negligible.

Accuracy of Results

Analysis of the sources of error and correlation of test data for duplicate conditions indicated the maximum probable errors in the data were as follows:

β , deg	T_c	J	C_N
± 0.15	± 0.002	± 0.01	± 0.004

By simple resolution of these forces, the blade-section force in the plane of the propeller (torque-producing force) becomes

$$f_Q = \frac{1}{2} \rho W^2 b (c_l \sin \phi + c_d \cos \phi) \quad (3)$$

The resultant velocity can be written as

$$W = \frac{V' \cos A' + V_a}{\sin \phi} \quad (4)$$

By the relationship of the resultant interference velocity to the axial interference velocity, that is,

$$V_i = \frac{V_a}{\cos \phi}$$

equation (4) for the resultant velocity becomes

$$W = \frac{V' \cos A' + V_i \cos \phi}{\sin \phi} \quad (5)$$

When equation (5) is used and $\tan \gamma = c_d/c_l$ is introduced, equation (3) for the torque-producing force becomes

$$f_Q = \frac{1}{2} \rho b c_l \frac{(V' \cos A' + V_i \cos \phi)^2}{\sin \phi} (1 + \tan \gamma \cot \phi) \quad (6)$$

which may be written in coefficient form as

$$c_{f_Q} = c_l \left(\frac{V'}{V} \right)^2 \frac{\cos^2 A'}{\sin \phi} \left(1 + \frac{V_i \cos \phi}{V' \cos A'} \right)^2 (1 + \tan \gamma \cot \phi) \quad (7)$$

The aerodynamic excitation of the propeller blades, due to the angle of upflow A' , is essentially sinusoidal in character and peaks at $\Omega = 90^\circ$ and $\Omega = 270^\circ$. If it is assumed that the propeller blade is operating far below resonance in first-mode bending, the oscillating thrust and torque force due to A' are also sinusoidal and in phase with the aerodynamic disturbance. It then follows that the amplitude of the once-per-revolution torque-producing force is given by

$$f_{Q1XP} = \frac{1}{2} (f_{Q\Omega=90} - f_{Q\Omega=270}) \quad (8)$$

The relationship between the normal force and the torque-producing force is

$$f_n = f_Q \sin \Omega$$

from which the average section normal force per blade per revolution can be expressed as

$$f_n = \frac{1}{2} f_{Q1XP} = \frac{1}{4} (f_{Q\Omega=90} - f_{Q\Omega=270}) \quad (9)$$

and the average total normal force for the propeller becomes

$$N = \frac{B}{4} \int_{r_s}^{R_t} (f_{Q\Omega=90} - f_{Q\Omega=270}) dr \quad (10)$$

Since by definition $C_N = N/qS$ and $x = r/R_t$, the equation for propeller normal-force coefficient can then be expressed in the form

$$C_N = \frac{B}{4\pi R_t} \int_{x_s}^{1.0} [(c_{f_Q})_{\Omega=90} - (c_{f_Q})_{\Omega=270}] b dx \quad (11)$$

The magnitude of c_{f_Q} can be calculated from equation (7) using any suitable method of evaluating the induction effects. In the present development two methods have been employed: The first method makes use of Goldstein's constant for lightly loaded propellers having minimum induced energy loss; the second method relies on an application of Theodorsen's circulation function and is more general in that an arbitrary blade loading can be considered. In the application of Goldstein's theory, equation (7) is modified by the basic assumption (ref. 6) that

$$\tan \alpha_1 = \frac{\sigma c_l}{4K \sin \phi} = \frac{V_1}{W}$$

From the geometry of the velocity diagram, the following expression may be stated:

$$(\cot \phi + \tan \alpha_1) = \frac{\cot \phi_0}{1 + \frac{V_1 \cos \phi}{V' \cos A'}}$$

Since, by definition $\sigma = \frac{Bb}{2\pi r}$ equation (7) can be written as

$$c_{f_Q} = K \frac{8\pi r}{Bb} \left(\frac{V'}{V}\right)^2 \cos^2 A' \left(\frac{\alpha_1}{57.3}\right) \left(\frac{\cot \phi_0}{\cot \phi + \frac{\alpha_1}{57.3}}\right)^2 \left(1 + \tan \gamma \cot \phi\right) \quad (12)$$

The Goldstein factor K is given in reference 6. Equation (12) was presented in reference 7 in slightly different form.

Application of Theodorsen's theory to equation (7) is accomplished by relating the resultant interference velocity to the rearward displacement velocity. From the geometry of the velocity diagram this relationship is given by

$$V_1 = \frac{1}{2} W \cos \phi$$

Defining $\bar{w} = w/V' \cos A'$ the foregoing expression becomes

$$V_1 = \frac{\bar{w}}{2} V' \cos A' \cos \phi$$

By substitution of this relation in equation (7), the coefficient of section torque-producing force becomes

$$c_{fQ} = c_l \left(\frac{V'}{V} \right)^2 \frac{\cos^2 A'}{\sin \phi} \left(1 + \frac{\bar{w}}{2} \cos^2 \phi \right)^2 \left(1 + \tan \gamma \cot \phi \right) \quad (13)$$

wherein the dimensionless parameter \bar{w} is related to Theodorsen's circulation function (ref. 9).

For the present calculations \bar{w} was evaluated with the use of reference 10, wherein this parameter is presented as a function of blade loading and advance ratio. In determining \bar{w} , values of advance ratio for the propeller uninclined were used. This assumption implies that the interference velocity is dependent on the element blade loading for the condition of propeller uninclined, but does not preclude use of instantaneous blade position for the determination of blade-section angle of attack. In determination of the blade-section angles of attack, the blade twist due to the combined effects of centrifugal force and steady loading was accounted for. A more rigorous solution should include the blade twist due to the oscillating air loads, and also any effect of blade vibration on either the instantaneous blade angle or on the phase lag between the LXP excitation and the resulting blade forces for conditions in which LXP resonance is approached.

Reference 11 was the source of the two-dimensional data for NACA 16-series airfoils used in performing the calculations. Reference 12 was used for obtaining the radial distribution of upflow angle, and the radial distribution of velocity was calculated by the following cubic equation:

$$\frac{V'}{V} = 1.0 + 0.08 \left(\frac{1-x}{1-x_s} \right)^3$$

RESULTS

The results of this investigation are presented in figures 4 through 10. In figures 4 and 5 the thrust characteristics of the propellers are shown. The normal-force characteristics are presented in figures 6 and 7 as a function of thrust coefficient and in figures 8 and 9 as a function of upflow angle at the 0.7 propeller radius. A comparison of the normal-force coefficient as determined from theory and experiment is shown in figures 8(b), 9 and 10.

DISCUSSION

Variation with Thrust

The basic normal-force data as presented in figure 6 indicate that for the thin propeller, the normal-force coefficient generally increased slightly with increasing thrust coefficient at Mach numbers below 0.70 and remained essentially constant at higher Mach numbers. The low-speed data for the thicker propeller (fig. 7) indicate that the normal-force coefficient generally increased with increasing thrust coefficient, the effect becoming more pronounced with increasing angle of attack.

Effect of Inclination

Propeller normal-force coefficient is shown as a function of upflow angle at the 0.7 propeller radius in figure 8 for the thin propeller, and in figure 9 for the thicker propeller. The angle of upflow at the propeller disk differs from the angle of attack of the thrust axis by the upwash induced by the spinner and nacelle. The relationship between the measured upflow angle and the angle of attack of the thrust axis has been determined from the data of reference 12 and is as follows:

M	$\frac{dA}{d\alpha}$
0.082 to .60	1.185
.70	1.174
.80	1.144
.83	1.130
.86	1.120
.90	1.100

For the thin propeller, the increase in normal-force coefficient with upflow angle was essentially linear (fig. 8). It is also seen from this figure that the slope of the normal-force curves is slightly reduced with increasing Mach number and slightly increased with increasing blade angle. The trend of normal-force coefficient with upflow angle for the thicker propeller was essentially linear, the greatest deviation from linearity occurring at a thrust coefficient of 0.6 for a blade angle of 21° (fig. 9). In addition, as previously noted for the thin propeller, the effect of increasing blade angle was an increase in the normal-force coefficient.

Comparison with Theory

It has been stated earlier in the report that the calculation of normal force for a high-speed condition (thin propeller) was performed by the method in which the induction effects are accounted for by Goldstein theory. The excellent agreement afforded by this method is shown in figure 8(b) for a blade angle of 51° and a Mach number of 0.70. This agreement might have been anticipated because the condition is one for which the loading was light and the lift distribution nearly optimum and, therefore, the loading did not violate the restriction of the Goldstein theory.

For conditions of low blade angle and low forward speed (thick propeller), the normal force was calculated by use of the method which accounts for induction effects by Theodorsen's circulation functions. In figure 9 the calculated values have been plotted at the values of upflow angle for which the calculations were made, and to the first order may be linearly extrapolated to zero upflow angle. It is apparent that the effect of thrust-axis inclination on normal-force coefficient was consistently underestimated by the theoretical method. A more comprehensive comparison is made in figure 10, wherein normal-force coefficient is given as a function of blade angle and also as a function of thrust coefficient. It is evident that the variation of normal-force coefficient with blade angle and thrust coefficient was predicted with fair accuracy, but that the absolute magnitude of the normal force was underestimated. The discrepancy between the magnitudes of the calculated and experimental values may be due to several possible sources of error. The first is the uncertainty of the two-dimensional airfoil data used in calculating the magnitude of the torque-producing force. The second is the assumed radial velocity gradient used in the absence of experimental data. Finally, the upflow angles, which were measured in the absence of the propeller, could conceivably have been larger with the propeller operating.

CONCLUDING REMARKS

Results of an investigation of the normal-force characteristics of the NACA 1.167-(0)(03)-058 and the NACA 1.167-(0)(05)-058 three-blade propellers showed that:

1. In general, the normal-force coefficient increased with increasing thrust coefficient at Mach numbers below 0.70 and remained essentially constant at the higher Mach numbers.
2. The increase in normal-force coefficient with upflow angle was essentially linear.

3. Increasing propeller blade angle increased the normal-force coefficient for a given value of thrust coefficient and angle of attack.

4. Comparison between the calculated normal force and that measured experimentally at a forward Mach number of 0.7 indicated excellent agreement.

5. At low forward speeds the theoretical method predicted the variation with thrust coefficient and blade angle of propeller normal force with fair accuracy, but consistently underestimated the effect of thrust-axis inclination.

Ames Aeronautical Laboratory
National Advisory Committee for Aeronautics
Moffett Field, Calif., Apr. 22, 1954

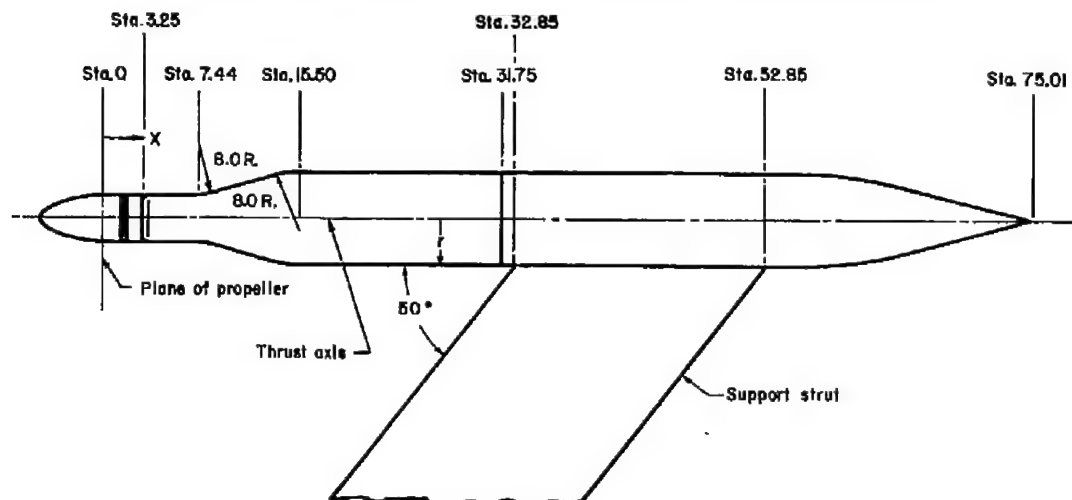
REFERENCES

1. Ribner, Herbert S.: Propellers in Yaw. NACA Rep. 820, 1945.
2. Demele, Fred A., and Otey, William R.: Investigation of the NACA 1.167-(0)(03)-058 and NACA 1.167-(0)(05)-058 Three-Blade Propellers at Forward Mach Numbers to 0.92 Including Effects of Thrust-Axis Inclination. NACA RM A53F16, 1953.
3. Herriot, John G.: Blockage Corrections for Three-Dimensional-Flow Closed-Throat Wind Tunnels, With Consideration of the Effect of Compressibility. NACA Rep. 995, 1950. (Formerly NACA RM A7B28)
4. Glauert, H.: The Elements of Aerofoil and Airscrew Theory. Cambridge, Eng. The Univ. Press; New York, Macmillan, 1943, pp. 222-226.
5. Young, A. D.: Note on the Application of the Linear Perturbation Theory to Determine the Effect of Compressibility on the Wind Tunnel Constraint on a Propeller. R. & M. No. 2113 (8301) British A.R.C., 1944. Also issued as: RAE Tech. Note Aero 1539, British, 1944.
6. Lock, C. N. H., and Yeatman, D.: Tables for Use in an Improved Method of Airscrew Strip Theory Calculation. R. & M. No. 1674, British A.R.C., 1935.

7. Sutton, Fred B., and Demele, Fred A.: The Effects of Operating Propellers on the Longitudinal Characteristics at High Subsonic Speeds of a Four-Engine Tractor Airplane Configuration Having a Wing With 40° of Sweepback and an Aspect Ratio of 10. NACA RM A53J23, 1954.
8. Lock, C. N. H.: An Application of Prandtl Theory to an Airscrew. R.&M. No. 1521, British A.R.C., 1933.
9. Crigler, John L.: Application of Theodorsen's Theory to Propeller Design. NACA Rep. 924, 1949. (Supersedes NACA RM L8F30.)
10. Glover, L. S., and Borst, H. V., comps.: Application of Theodorsen's Theory to Strip Analysis Procedure For Single Rotation Propellers. Rep. No. C-2070, Curtiss-Wright Corp., Propeller Division. (Caldwell, N. J.), 1949.
11. Enos, L. H., and Borst, H. V.: Propeller Performance Analysis. Aerodynamic Characteristics, NACA 16 Series Airfoils. Pt. II. Rep. No. C-2000, Curtiss-Wright Corp., Propeller Division. (Caldwell, N. J.), 1948.
12. Lopez, Armando E., and Dickson, Jerald K.: The Effects of Compressibility on the Upwash at the Propeller Planes of a Four-Engine Tractor Airplane Configuration Having a Wing With 40° of Sweepback and an Aspect Ratio of 10. NACA RM A53A30a, 1953.

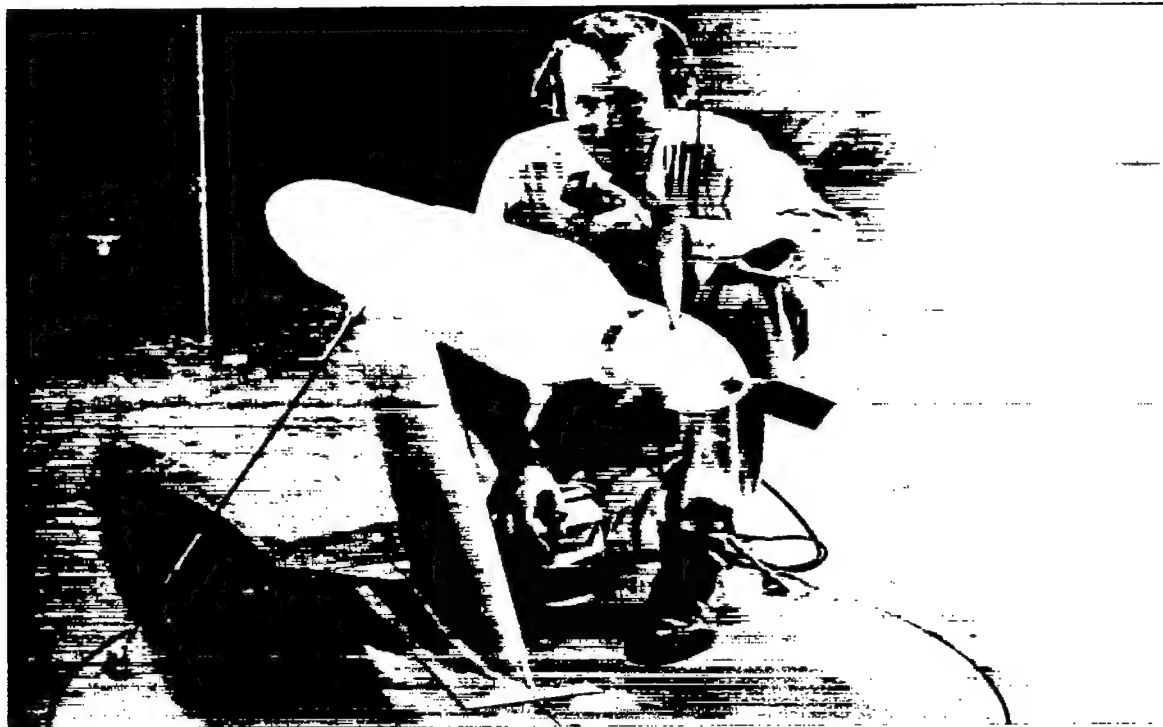
TABLE I.- COORDINATES OF NACELLE ASSEMBLY

[All dimensions in inches unless otherwise noted]



Distance from propeller plane, x	Radius from thrust axis, r	Distance from propeller plane, x	Radius from thrust axis, r	Distance from propeller plane, x	Radius from thrust axis, r
-5.00	0	0	1.985	59.60	3.25
-4.79	.385	2.00	2.100	61.60	3.04
-4.58	.567	7.44	2.100	63.60	2.74
-4.25	.788	15.50	3.750	65.60	2.36
-3.95	.951	31.75	3.750	67.60	1.91
-3.25	1.242	32.00	3.500	69.60	1.41
-2.55	1.472	53.60	3.500	71.60	.91
-1.80	1.670	55.60	3.470	73.60	.38
-.80	1.871	57.60	3.390	75.01	0





A-18567

Figure 1.- Photograph of the nacelle assembly.

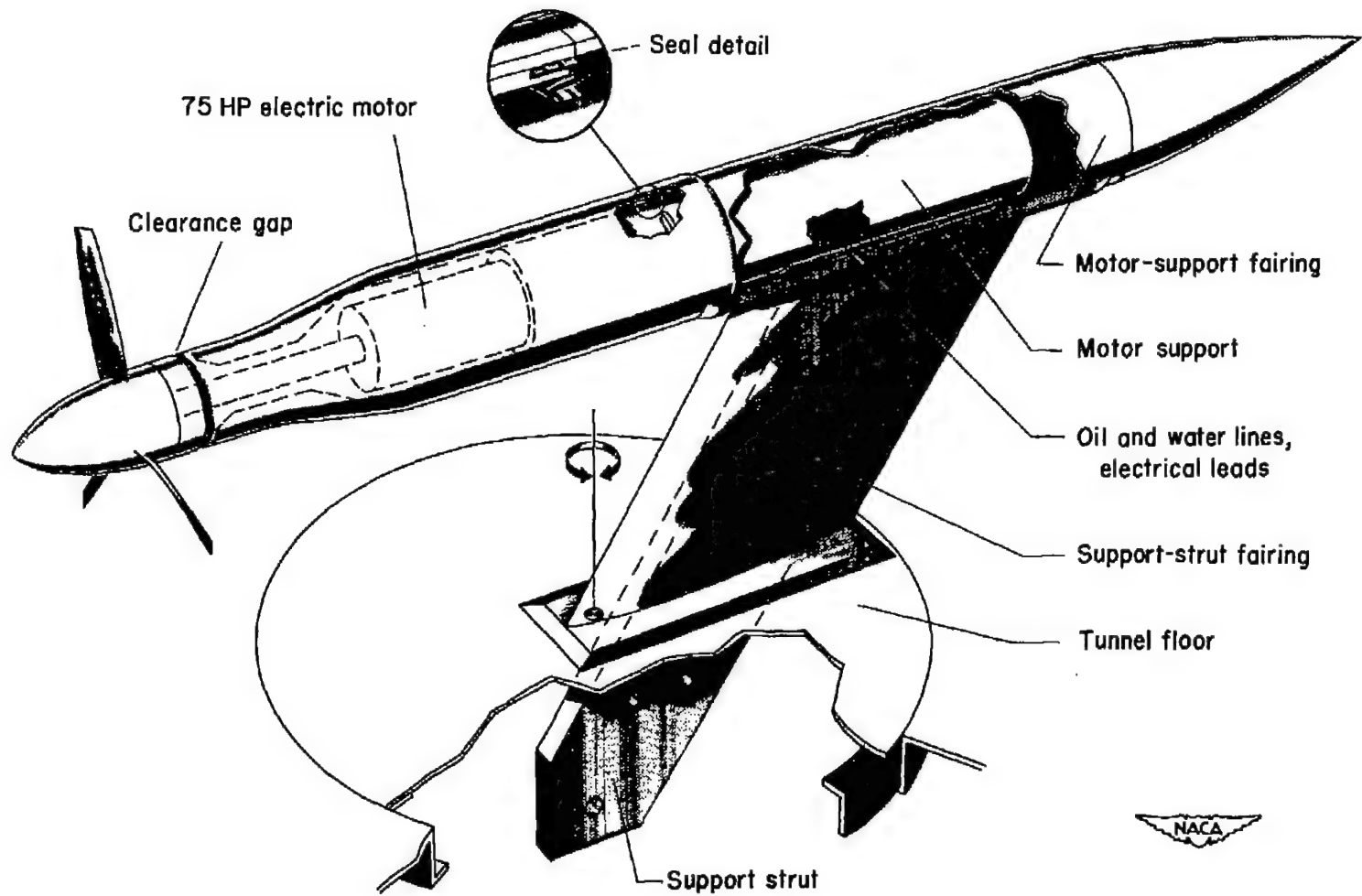


Figure 2.- Nacelle assembly.

Developed plan form

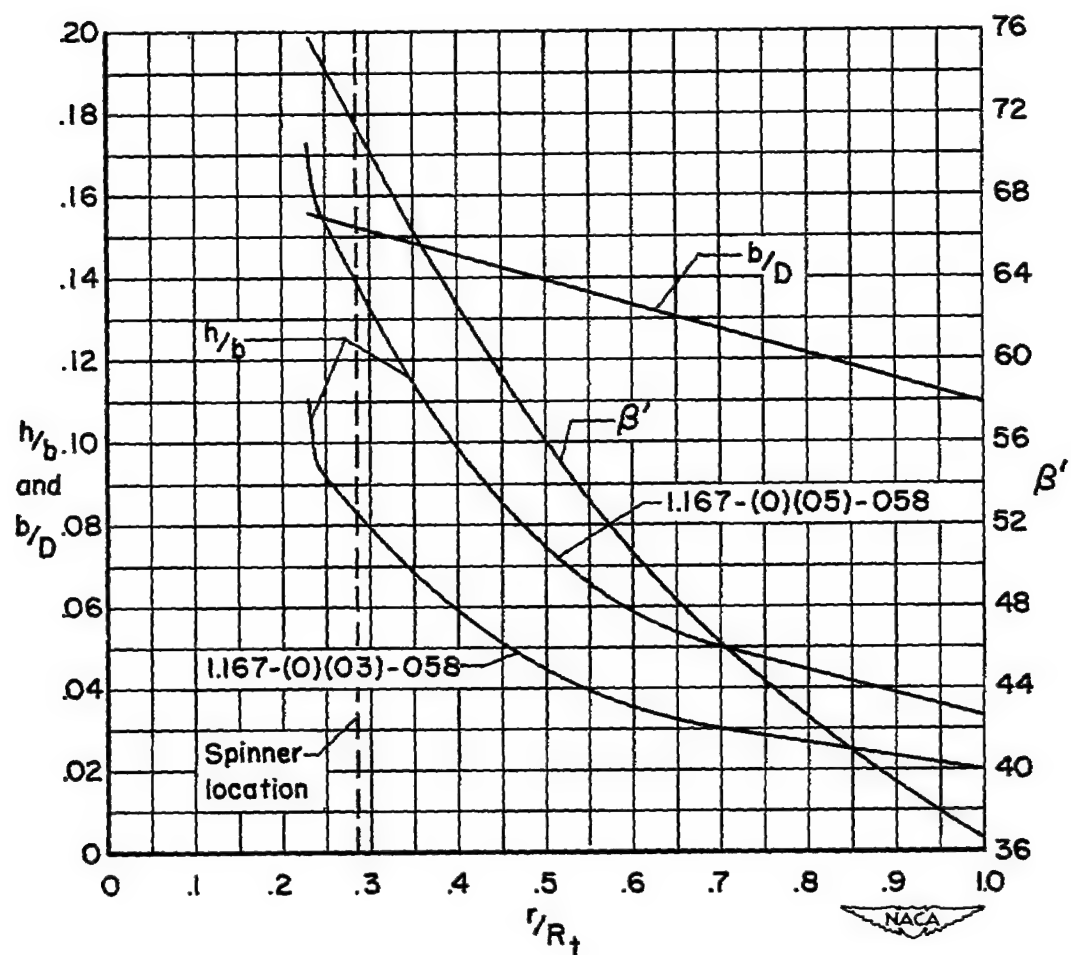
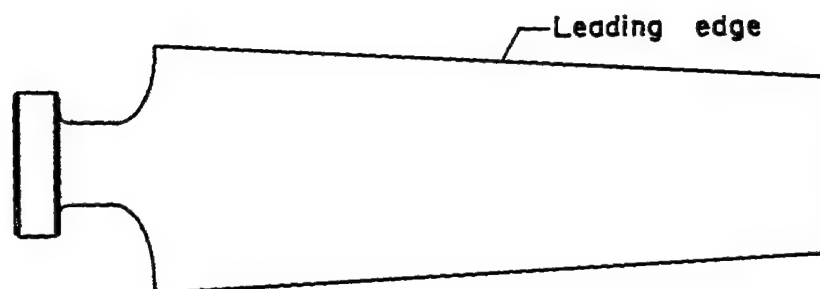


Figure 3.- Blade-form curves for the NACA 1.167-(0)(03)-058 and the NACA 1.167-(0)(05)-058 three-blade propellers.

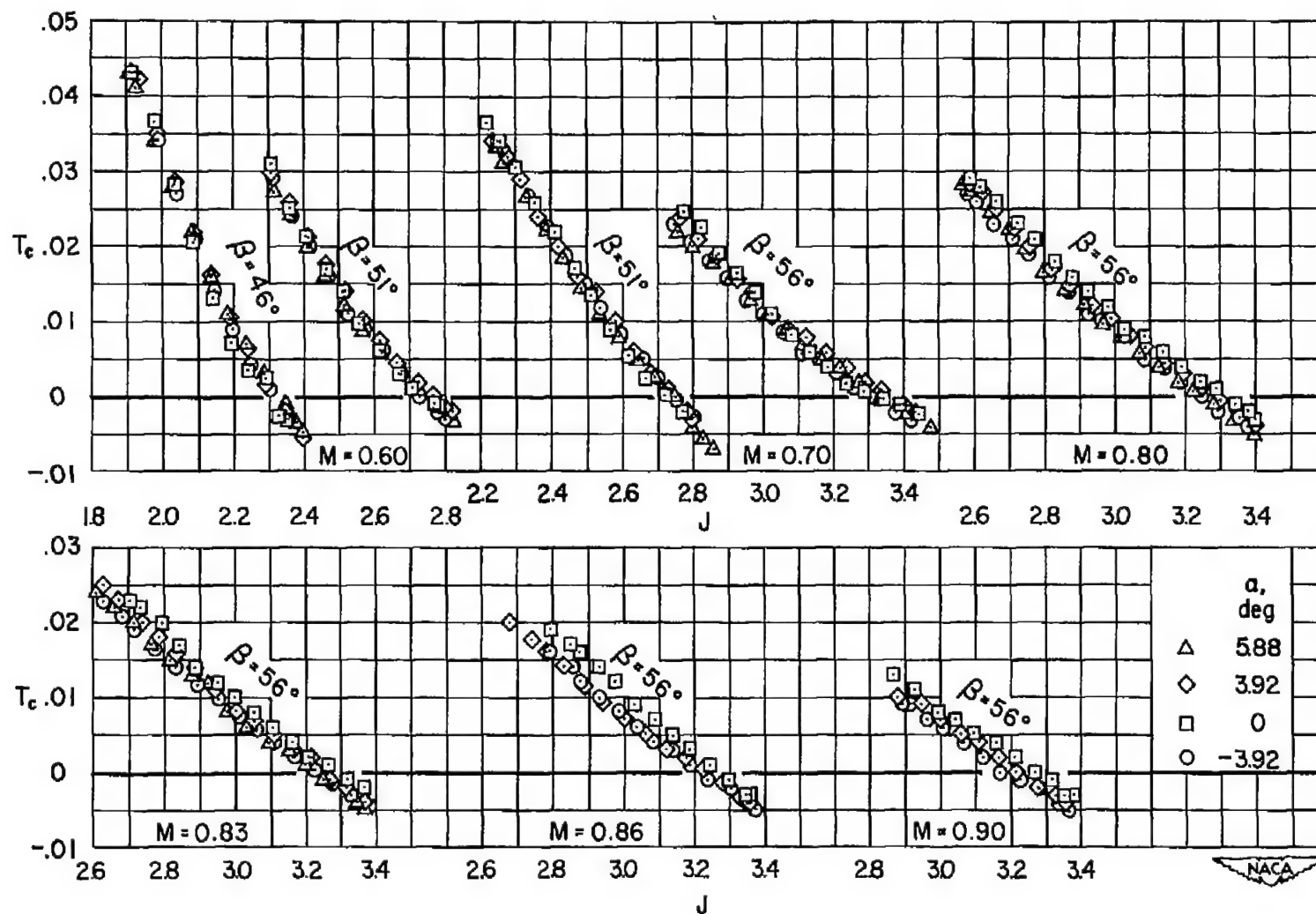


Figure 4.- Thrust characteristics of the NACA 1.167-(0)(03)-058 propeller; $R = 1,600,000$.

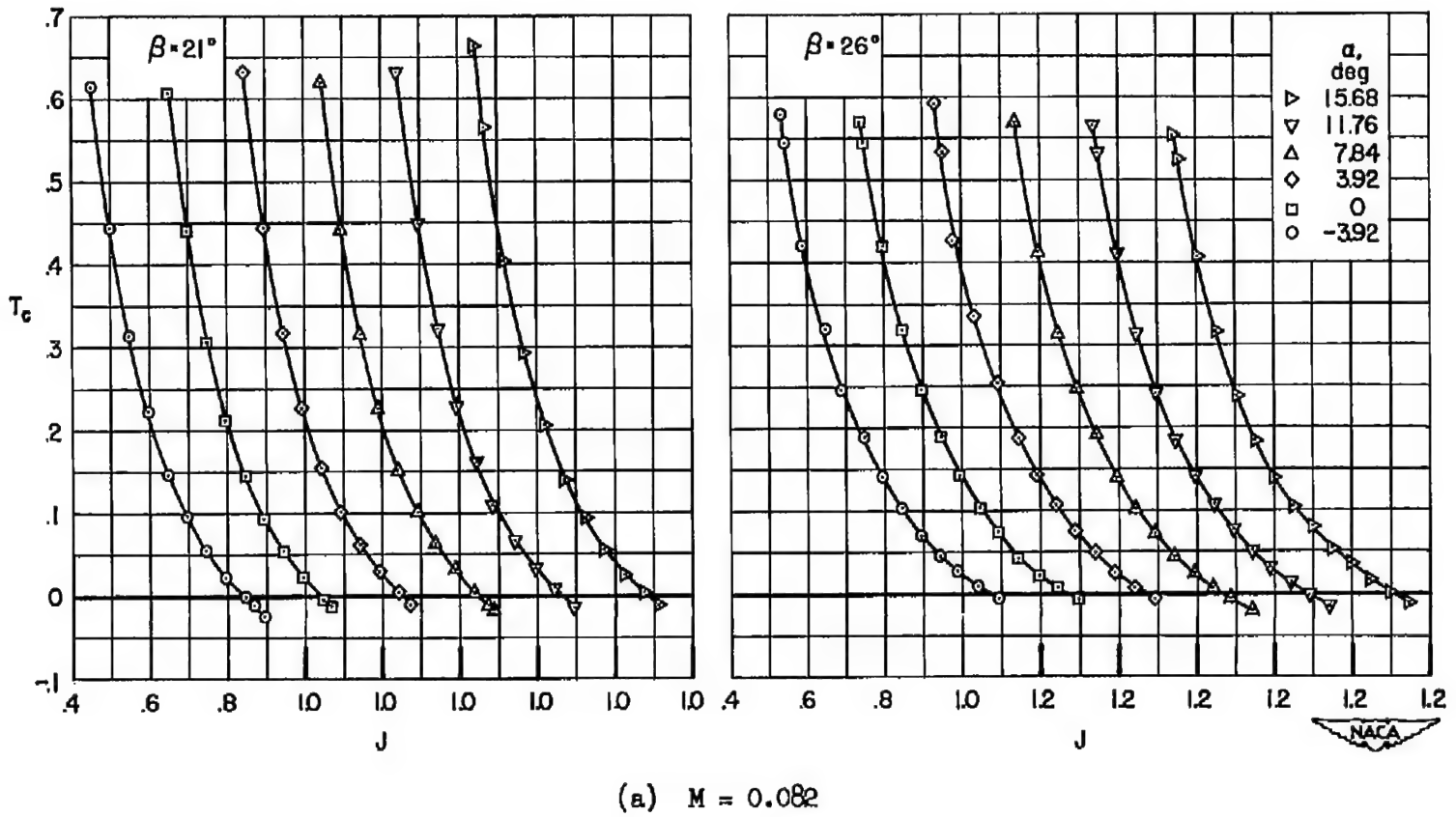
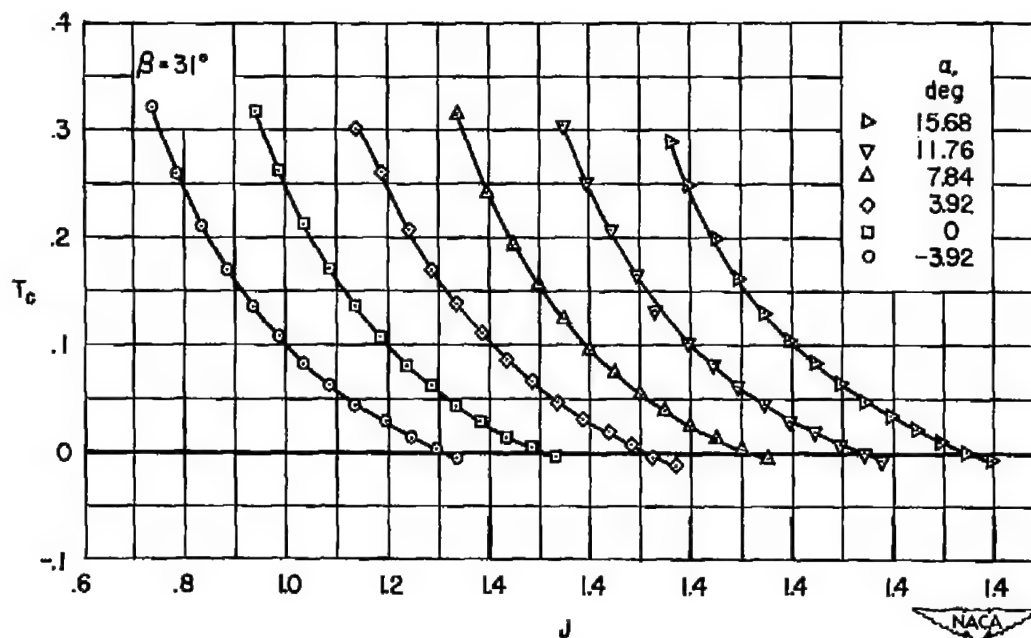
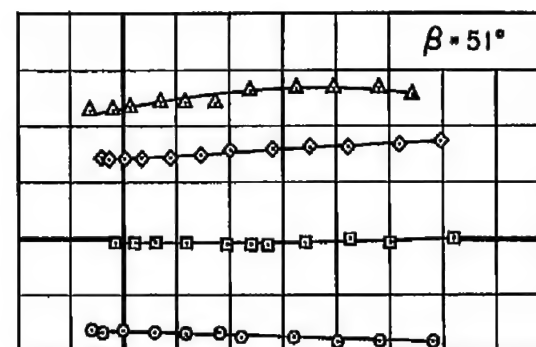
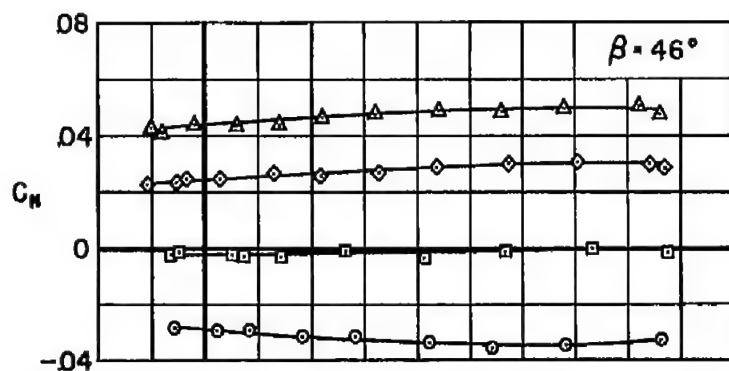
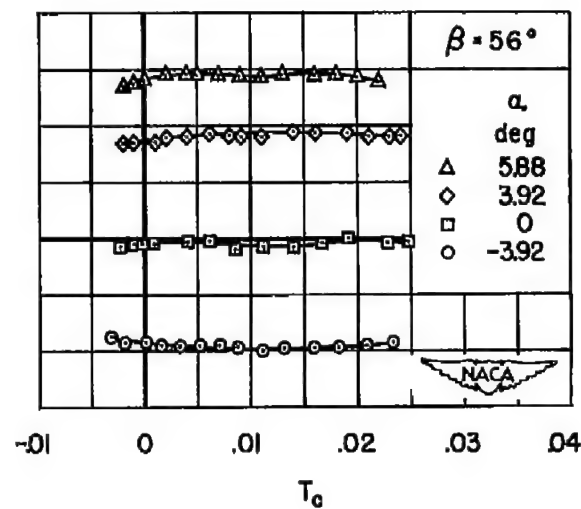
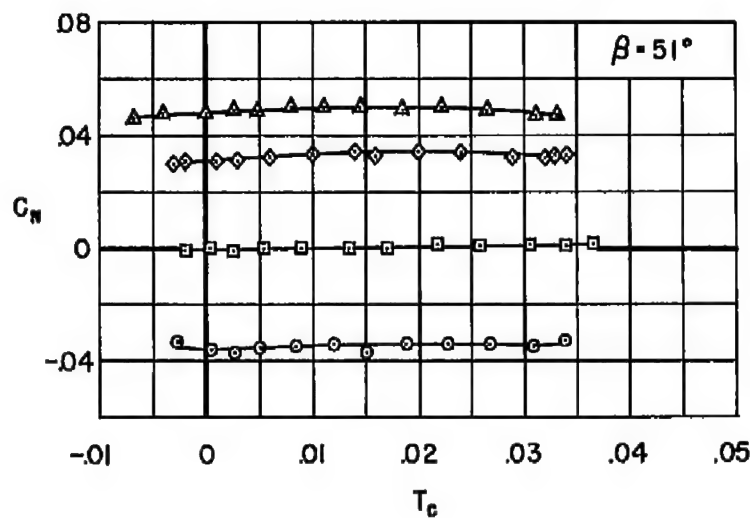


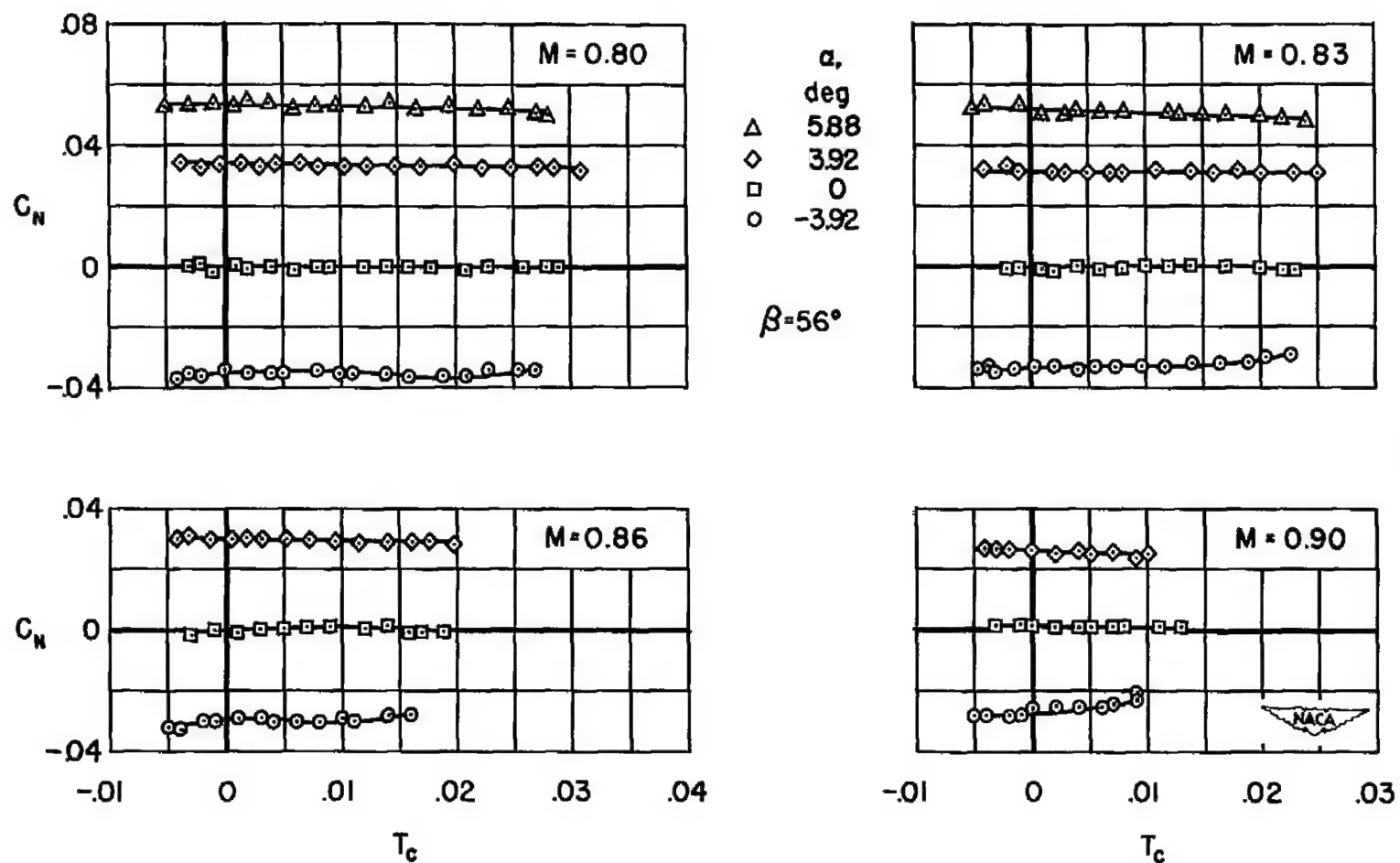
Figure 5.- Thrust characteristics of the NACA 1.167-(0)(05)-058 propeller; $R = 3,200,000$.



(b) $M = 0.123$

Figure 5.- Concluded.

(a) $M = 0.60$ (b) $M = 0.70$ Figure 6.- Normal-force characteristics of the NACA 1.167-(0)(03)-058 propeller; $R = 1,600,000$.



(c) $M = 0.80, 0.83, 0.86, 0.90$

Figure 6.- Concluded.

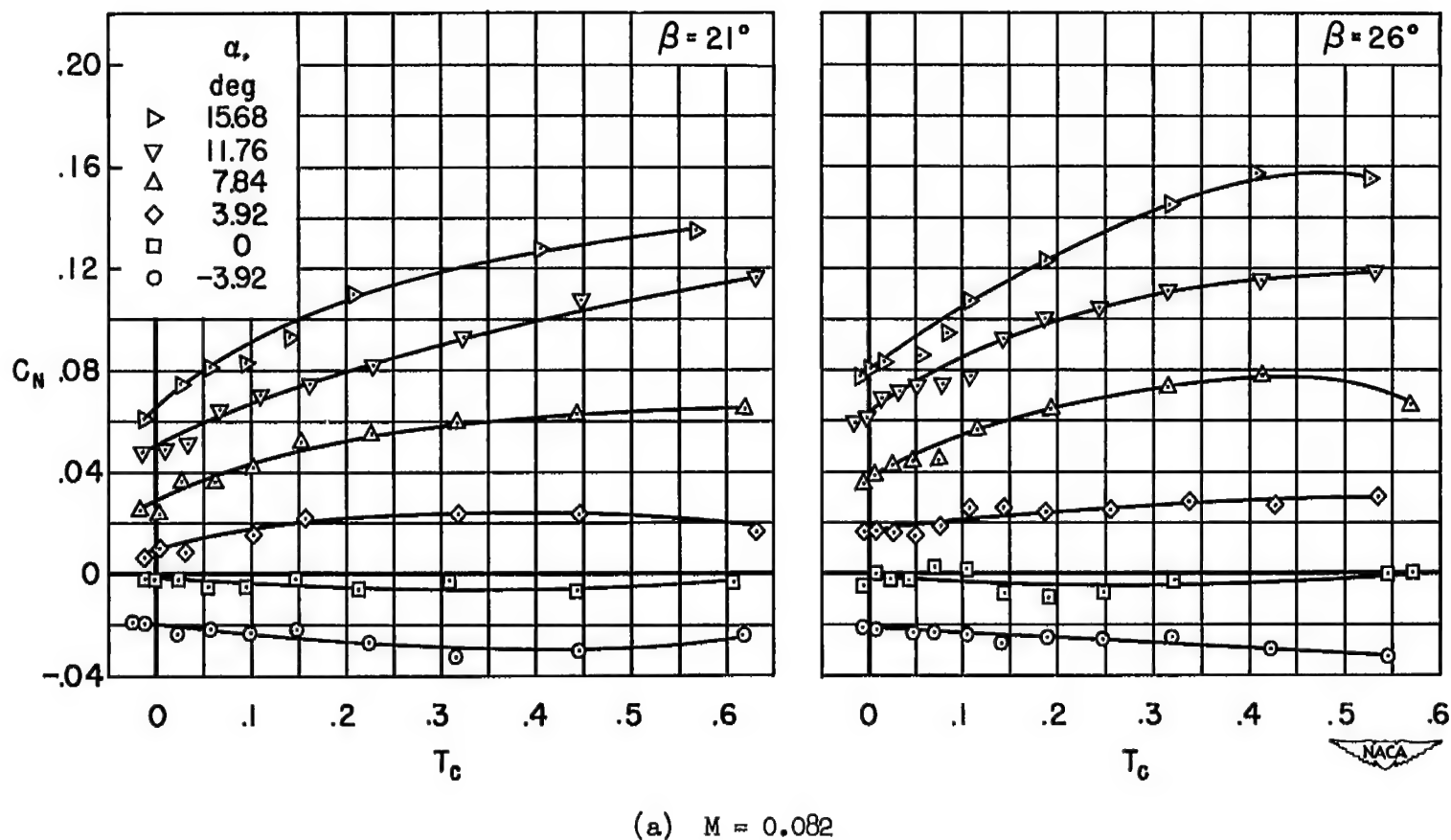
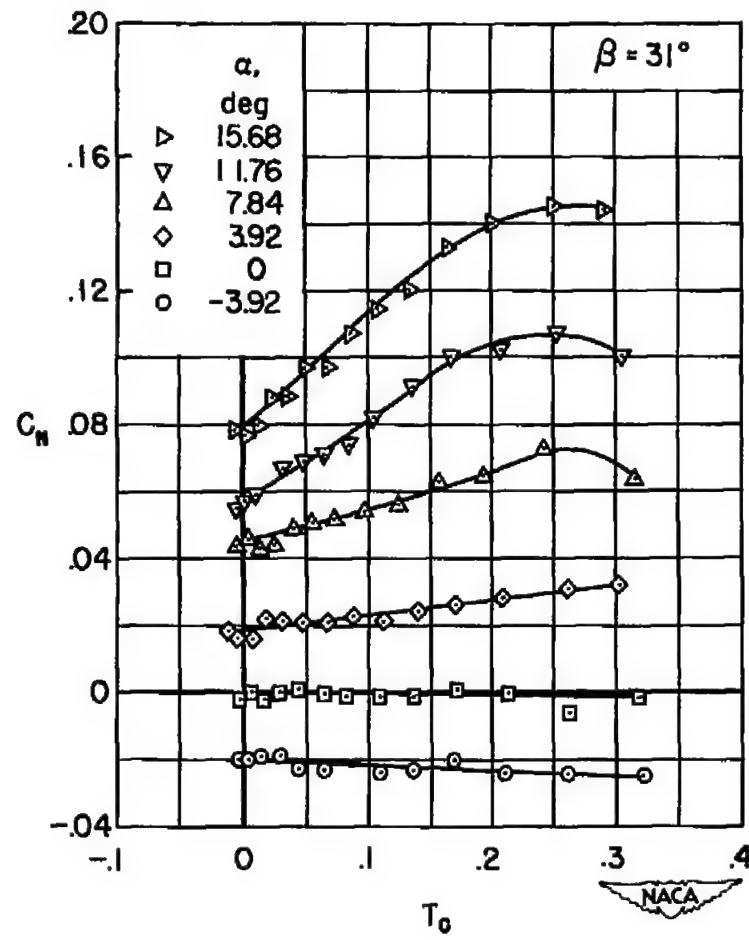


Figure 7.-- Normal-force characteristics of the NACA 1.167-(0)(05)-058 propeller; $R = 3,200,000$.



(b) $M = 0.123$

Figure 7.- Concluded.

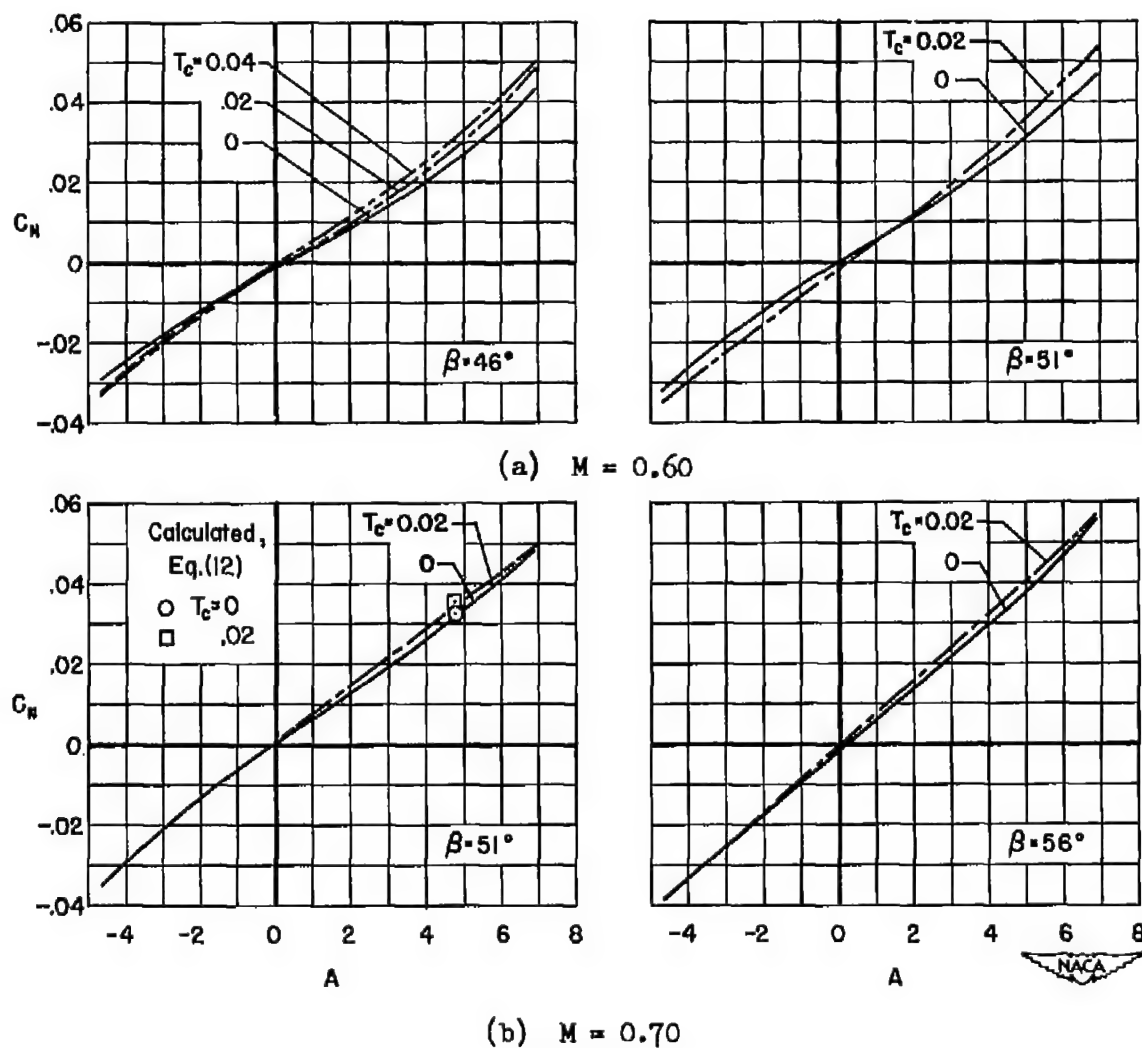
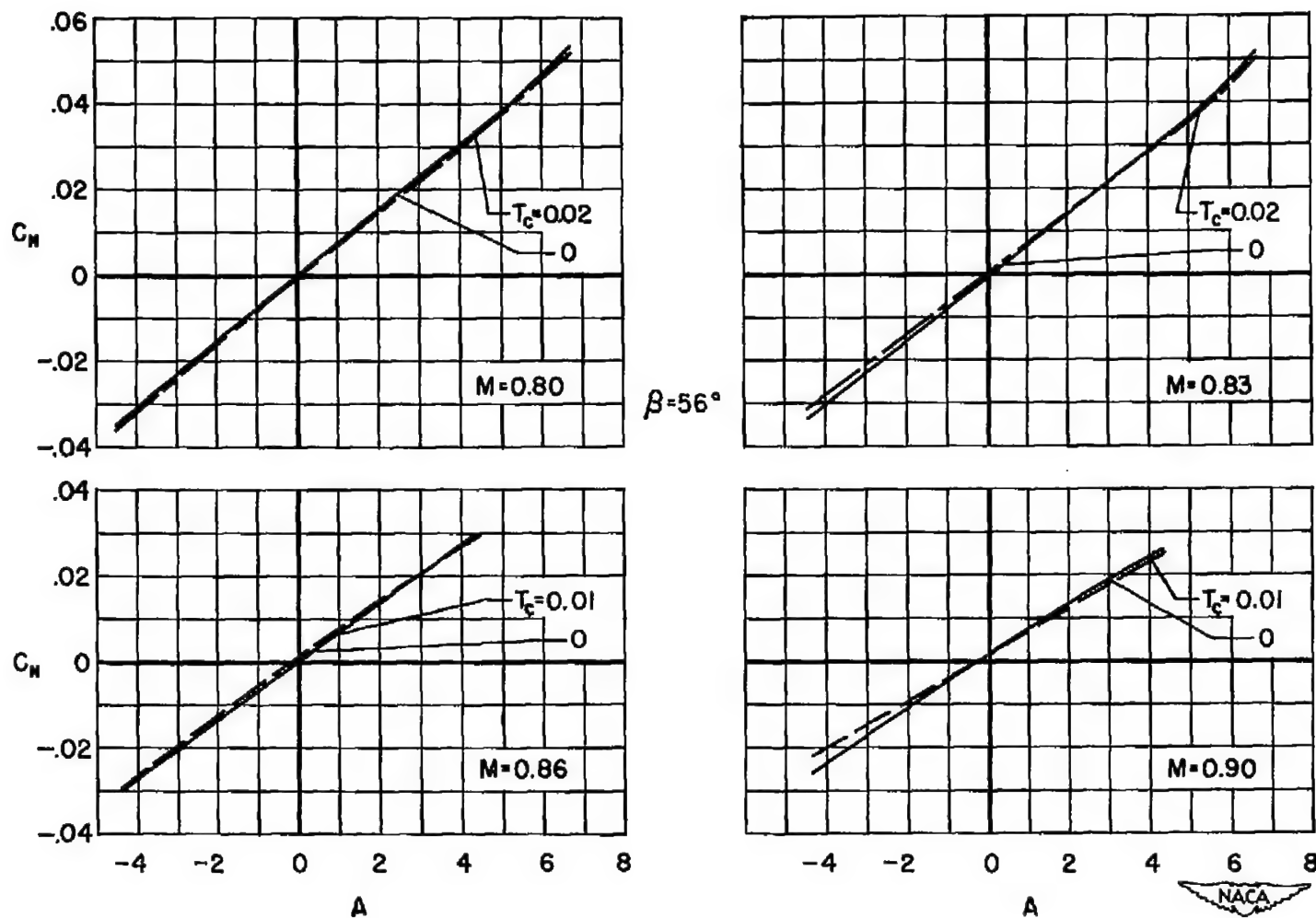


Figure 8.- The variation of normal-force coefficient with upflow angle for the NACA 1.167-(0)(03)-058 propeller; $R = 1,600,000$.



(c) $M = 0.80, 0.83, 0.86, 0.90$

Figure 8.- Concluded.

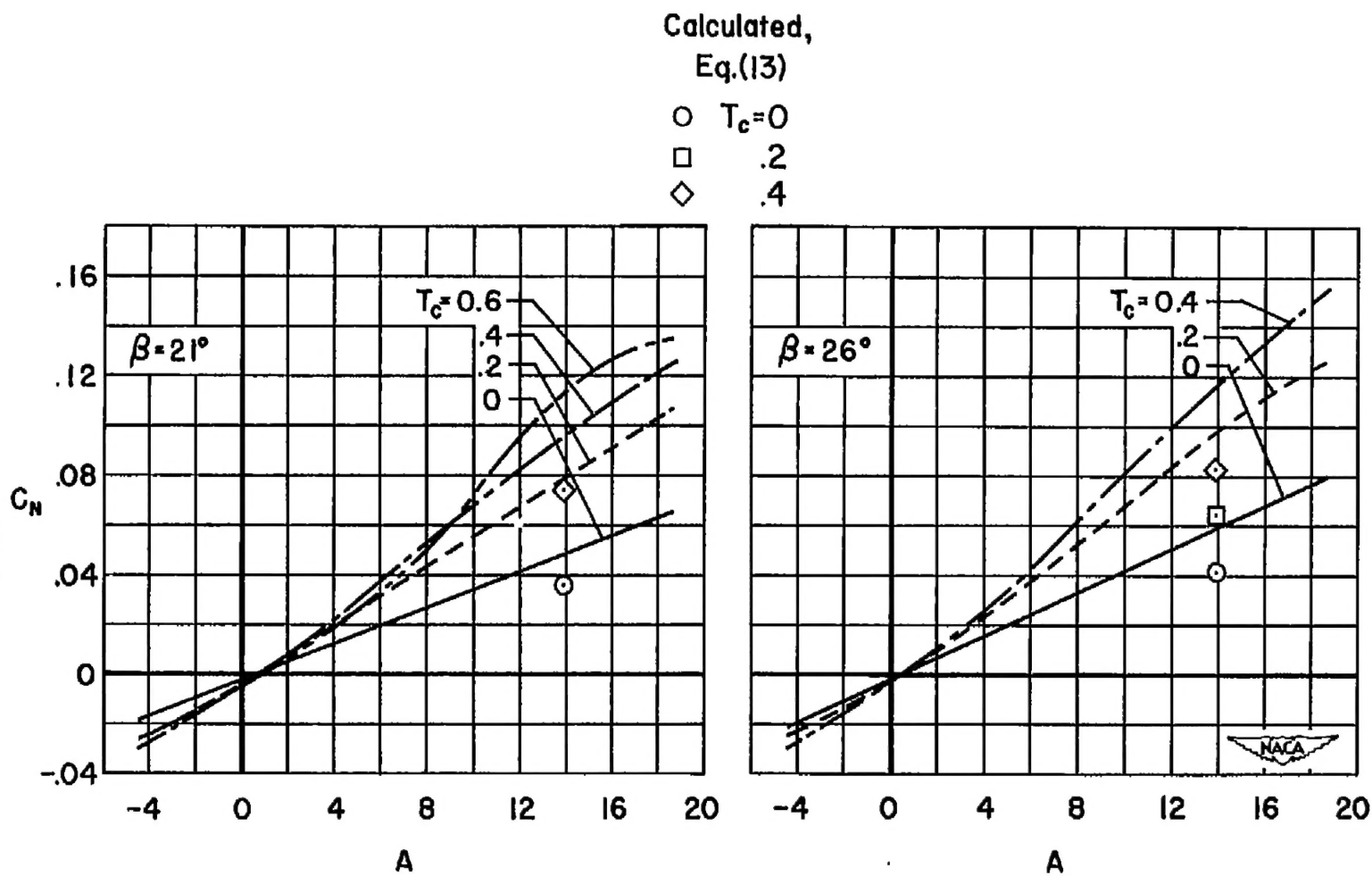
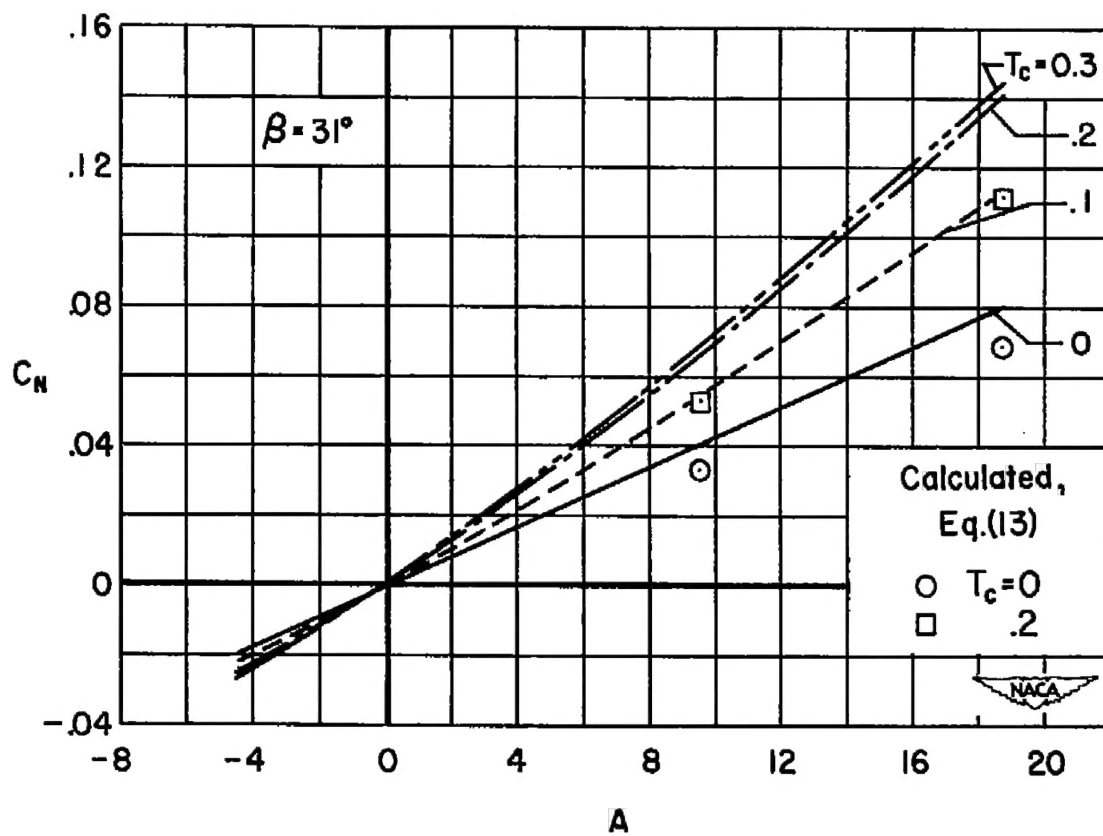


Figure 9.- The variation of normal-force coefficient with upflow angle for the NACA 1.167-(0)(05)-058 propeller; $R = 3,200,000$.



(b) $M = 0.123$

Figure 9.- Concluded.

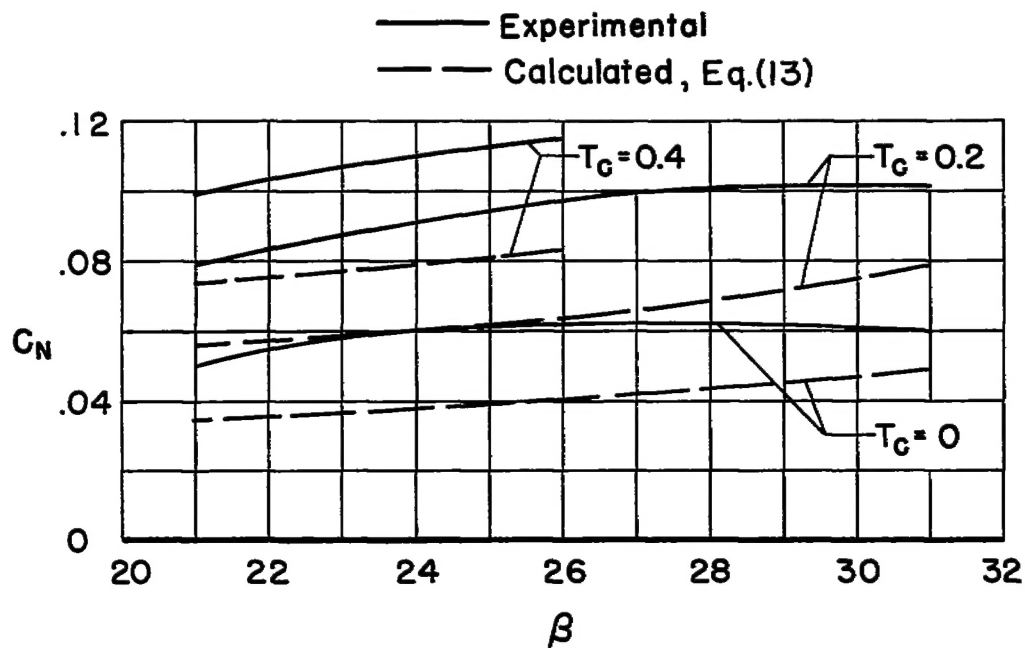
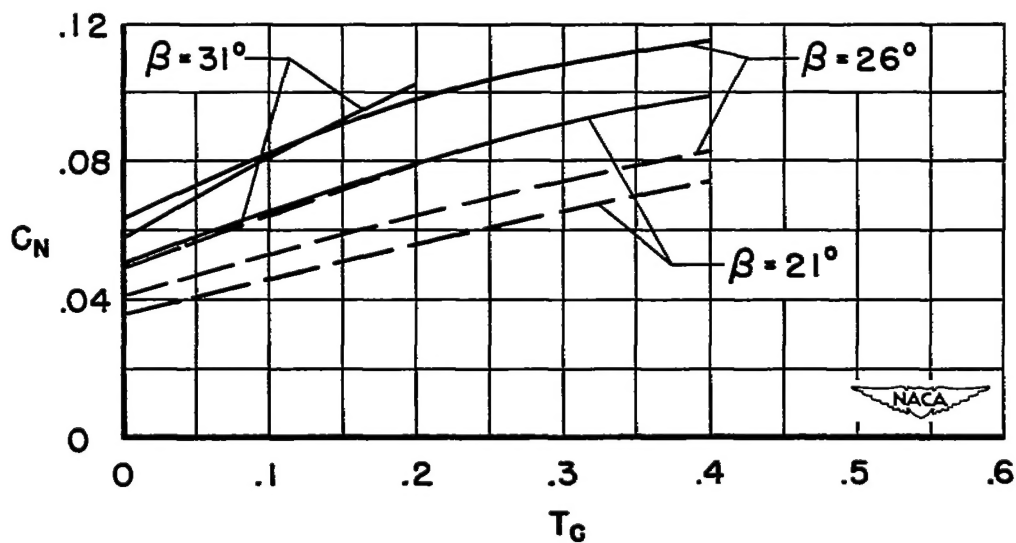
(a) C_N vs. β (b) C_N vs. T_C

Figure 10.- Correlation between calculated and experimental values of normal-force coefficient for the NACA 1.167-(0)(05)-058 propeller at low forward speed; $\alpha = 11.76^\circ$; $A = 13.9^\circ$.

~~CONFIDENTIAL~~

CONFIDENTIAL



CONFIDENTIAL